Short-range ordering of oxygen vacancies in $CaFe_xTi_{1-x}O_{3-x/2}$ perovskites ($0 < x < 0.4$)



2000 J. Phys.: Condens. Matter 12 2969

(http://iopscience.iop.org/0953-8984/12/13/308)

J. Phys.: Condens. Matter **12** (2000) 2969–2984. Printed in the UK PII: S0953-8984(00)09447-9

# Short-range ordering of oxygen vacancies in $CaFe_xTi_{1-x}O_{3-x/2}$ perovskites ($0 < x < 0.4$)

C A McCammon†, A I Becerro†, F Langenhorst†, R J Angel†, S Marion‡ and F Seifert†

† Bayerisches Geoinstitut, Universität Bayreuth, D-95440 Bayreuth, Germany
‡ Centre for Materials Science, University of Oslo, N-0349 Oslo, Norway

E-mail: Catherine.McCammon@uni-bayreuth.de, Ana-Isabel.Becerro@uni-bayreuth.de, Falko.Langenhorst@uni-bayreuth.de, Ross.Angel@uni-bayreuth.de, Stefan.Marion@kjemi.uio.no and Friedrich.Seifert@uni-bayreuth.de

Received 10 November 1999

**Abstract.** We have synthesized samples in the system $CaTi_{1-x}Fe_xO_{3-x/2}$ with $x = 0.05$–$0.38$ at temperatures of 900–1320 °C under controlled conditions of oxygen fugacity. After drop quenching, samples were characterized by x-ray diffraction, transmission electron microscopy (TEM) and Mössbauer spectroscopy. Electrical conductivity measurements were made as a function of temperature, oxygen fugacity and sample composition. X-ray diffraction showed no long-range ordering of oxygen vacancies, which was confirmed by TEM measurements. Mössbauer spectroscopy showed Fe occurring in octahedral, tetrahedral and pentacoordinated sites. Analysis of area ratios indicates that a small number of Ti atoms must be located on non-octahedral sites, where the relative proportion of Ti on these sites decreases with increasing concentration of oxygen vacancies. Results are interpreted in terms of a model for short-range ordering of oxygen vacancies where clusters form chains of increasing length. The structure is dominated by oxygen vacancy monomers at low Fe concentrations, and the average number of vacancies per chain increases with increasing Fe concentration. Results are consistent with conductivity results which show high ionic conductivity at moderately low Fe concentrations.

## 1. Introduction

The ability of the perovskite structure to incorporate more than half of the stable elements in the periodic table in its crystal structure leads to a wealth of interesting properties, including many that involve a departure from the general formula $ABO_3$. Anion vacancies can be formed by substitution of cations with different valence, for example substitution of $Fe^{3+}$ for $Ti^{4+}$ in $CaTiO_3$, and both the abundance and arrangement of these anion vacancies can have profound effects on physical properties. For example, Iwahara *et al* (1988) report high ionic conductivities in $CaTi_{1-x}Fe_xO_{3-y}$ that are dependent on the concentration and mobility of oxygen vacancies. Marion *et al* (2000) reported a discontinuity in the electrical conductivity of $CaTi_{0.8}Fe_{0.2}O_{3-y}$ spanning nearly one order of magnitude, which could be attributed to an order–disorder transition involving oxygen vacancies. N L Ross (personal communication, 1998) found that the bulk modulus of $CaFeO_{2.5}$ is some 25% less than would be predicted from volume–bulk modulus systematics in stoichiometric perovskites. In this paper we focus on the system $CaTiO_3$–$CaFeO_{2.5}$ and the oxygen vacancy distribution inferred to exist at high temperatures.

0953-8984/00/132969+16$30.00  

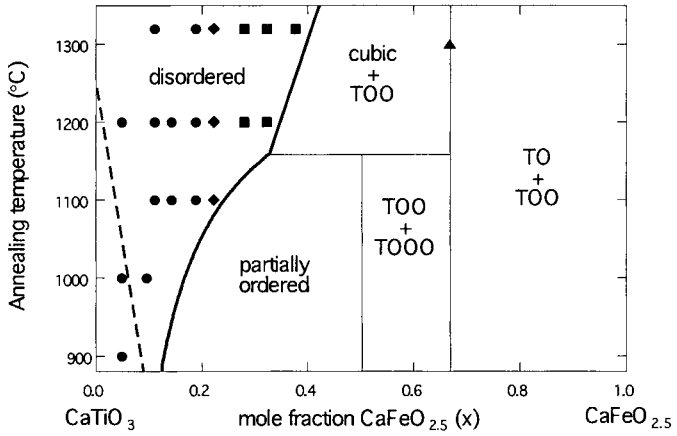


**Figure 1.** Structural state of perovskites in the system $CaTiO_3$–$CaFeO_{2.5}$ as a function of annealing temperature and composition. The symbols show the compositions studied using Mössbauer spectroscopy. The symmetry of the samples after quenching is as follows: circle = orthorhombic; diamond = tetragonal; square = cubic; triangle = orthorhombic (ordered). The dotted line indicates the displacive phase transition boundary, while the symbols TO, TOO and TOOO refer to the sequence of layers of tetrahedra and octahedra in the ordered structures (after Becerro *et al* 1999).

The phase diagram of $CaTiO_3$–$CaFeO_{2.5}$ has been described by Becerro *et al* (1999) (figure 1). In the region labelled 'disordered' there is no long-range ordering of oxygen vacancies in the perovskite structure. At moderate Fe contents and lower temperatures the vacancies are partially ordered into chains of infinite length (region labelled 'partially ordered'), while structures that are fully ordered with a regular sequence of octahedral (O) and tetrahedral (T) layers occur at $x = 0.5$ (TOOO structure, Hovmöller *et al* 1988), $x = 0.67$ (TOO structure, Rodríguez-Carvajal *et al* 1989) and $x = 1$ (TO structure, Colville 1970). In this paper we will consider only the disordered region.

There have been several studies into the nature of oxygen vacancies in the disordered region of the system $CaTiO_3$–$CaFeO_{2.5}$. Mössbauer spectroscopy is one of the most effective tools for such studies, because of its sensitivity to the immediate environment of the Fe atoms and its ability to distinguish between different valence states. Grenier *et al* (1981) summarize work from their group using Mössbauer spectroscopy and transmission electron microscopy (TEM), where a model for short-range ordering of oxygen vacancies is proposed based on the relative abundance of $Fe^{3+}$ in the two coordination states that they found: tetrahedral and octahedral. However, Becerro *et al* (1999) reported in preliminary work the presence of a significant amount of pentacoordinated $Fe^{3+}$ in the disordered region of the system $CaTiO_3$–$CaFeO_{2.5}$ that was not reported in any of the previous studies. Coordination of $Fe^{3+}$ is closely related to the arrangement of oxygen vacancies, so the system needs to be re-examined.

In this paper we report Mössbauer studies from samples synthesized over a range of compositions and annealing temperatures in the disordered region of the system $CaTiO_3$–$CaFeO_{2.5}$, which, combined with results from TEM and electrical conductivity studies, provide a clearer picture of the nature of short-range ordering of oxygen vacancies.

## 2. Experimental methods

Polycrystalline samples in the system $CaTiO_3$–$CaFeO_{2.5}$ were synthesized from mixtures of $CaCO_3$, $TiO_2$ and $Fe_2O_3$ by slow decarbonatization and sintering at 1350 °C, followed by repeated intermittent grinding. These materials were then heated in open AgPd capsules

**Table 1.** Hyperfine parameters from room-temperature (293 K) Mössbauer spectra of $CaFe_xTi_{1-x}O_{3-x/2}$.

| | | | | Octahedral $Fe^{3+}$ | | | | Tetrahedral $Fe^{3+}$ | | | | Pentacoordinated $Fe^{3+}$ | | | |
|---|---|---|---|---|---|---|---|---|---|---|---|---|---|---|---|
| $T$ (°C) | Time[a] (h) | $x$ | Structure from XRD | $\delta$[b] (mm $s^{-1}$) | $\Delta E_Q$ (mm $s^{-1}$) | $\Gamma$ (mm $s^{-1}$) | $A$ (%) | $\delta$[b] (mm $s^{-1}$) | $\Delta E_Q$ (mm $s^{-1}$) | $\Gamma$ (mm $s^{-1}$) | $A$ (%) | $\delta$[b] (mm $s^{-1}$) | $\Delta E_Q$ (mm $s^{-1}$) | $\Gamma$ (mm $s^{-1}$) | $A$ (%) |
| 900 | 1660 | 0.048(4) | ortho | 0.33(1) | 0.22(5) | 0.60(12) | 54(6) | 0.17(2) | 1.51(4) | 0.43(7) | 17(4) | 0.27(2) | 0.94(3) | 0.42(6) | 29(6) |
| 1000 | 44 | 0.048(4) | ortho | 0.35(1) | 0.26(3) | 0.51(9) | 50(6) | 0.17(3) | 1.54(5) | 0.36(10) | 9(4) | 0.25(2) | 0.98(4) | 0.53(7) | 41(6) |
| | 44 | 0.096(56) | ortho | 0.35(2) | 0.37(3) | 0.55(6) | 58(5) | 0.17(1) | 1.50(1) | 0.29(2) | 21(3) | 0.27(2) | 0.94(3) | 0.42(7) | 21(5) |
| 1100 | 191 | 0.110(23) | ortho | 0.34(1) | 0.33(1) | 0.48(2) | 62(1) | 0.18(1) | 1.47(2) | 0.32(2) | 15(1) | 0.26(1) | 0.99(1) | 0.34(2) | 24(1) |
| | 191 | 0.142(7) | ortho | 0.36(1) | 0.34(2) | 0.47(2) | 55(1) | 0.18(1) | 1.47(2) | 0.34(2) | 17(1) | 0.27(1) | 0.98(1) | 0.36(2) | 28(1) |
| | 191 | 0.188(10) | ortho | 0.35(1) | 0.41(2) | 0.46(1) | 56(3) | 0.17(1) | 1.47(2) | 0.33(3) | 18(2) | 0.28(1) | 1.02(2) | 0.34(4) | 27(3) |
| | 191 | 0.222(15) | tetr | 0.36(1) | 0.48(1) | 0.45(1) | 50(1) | 0.17(1) | 1.51(1) | 0.32(1) | 25(1) | 0.29(1) | 1.01(1) | 0.39(3) | 25(2) |
| 1200 | 140 | 0.048(4) | ortho | 0.35(2) | 0.21(5) | 0.70(8) | 66(7) | 0.18(2) | 1.48(4) | 0.42(9) | 11(5) | 0.24(1) | 0.95(5) | 0.49(11) | 23(6) |
| | 140 | 0.110(23) | ortho | 0.33(1) | 0.32(1) | 0.50(3) | 68(2) | 0.19(1) | 1.44(3) | 0.29(4) | 13(2) | 0.25(1) | 0.99(2) | 0.30(3) | 20(2) |
| | 140 | 0.142(7) | ortho | 0.36(1) | 0.35(1) | 0.47(2) | 55(1) | 0.19(1) | 1.45(2) | 0.34(3) | 18(1) | 0.28(1) | 0.97(1) | 0.36(2) | 27(1) |
| | 140 | 0.188(10) | ortho | 0.37(1) | 0.41(2) | 0.47(3) | 53(3) | 0.19(1) | 1.50(2) | 0.32(3) | 18(2) | 0.28(1) | 1.02(2) | 0.36(4) | 29(3) |
| | 140 | 0.222(15) | tetr? | 0.37(1) | 0.43(3) | 0.42(4) | 42(5) | 0.19(1) | 1.51(2) | 0.36(3) | 23(3) | 0.31(1) | 0.96(3) | 0.40(6) | 34(5) |
| | 140 | 0.279(7) | cubic | 0.36(1) | 0.49(1) | 0.43(2) | 44(2) | 0.20(1) | 1.50(1) | 0.38(2) | 28(1) | 0.31(1) | 1.00(1) | 0.39(3) | 28(2) |
| | 140 | 0.322(18) | cubic | 0.37(1) | 0.55(1) | 0.42(1) | 43(2) | 0.19(1) | 1.51(1) | 0.37(1) | 31(1) | 0.32(1) | 1.03(1) | 0.38(3) | 26(2) |
| 1320 | 45 | 0.110(23) | ortho | 0.34(1) | 0.30(2) | 0.48(5) | 63(4) | 0.18(3) | 1.56(4) | 0.34(11) | 8(3) | 0.26(1) | 1.01(3) | 0.38(5) | 29(4) |
| | 40 | 0.188(10) | ortho | 0.36(1) | 0.40(1) | 0.44(2) | 52(1) | 0.18(1) | 1.47(1) | 0.34(2) | 20(1) | 0.28(1) | 1.00(1) | 0.35(2) | 28(2) |
| | 40 | 0.222(15) | tetr | 0.36(1) | 0.47(2) | 0.46(3) | 50(3) | 0.19(1) | 1.51(2) | 0.37(3) | 25(3) | 0.30(1) | 1.01(2) | 0.37(6) | 25(4) |
| | 40 | 0.279(7) | cubic | 0.36(1) | 0.51(2) | 0.45(2) | 47(3) | 0.19(1) | 1.52(2) | 0.39(2) | 27(2) | 0.31(1) | 1.01(2) | 0.37(4) | 26(3) |
| | 40 | 0.322(18) | cubic | 0.37(1) | 0.57(2) | 0.45(3) | 47(4) | 0.20(1) | 1.52(2) | 0.35(3) | 28(3) | 0.30(1) | 1.06(3) | 0.39(7) | 25(5) |
| | 40 | 0.376(28) | cubic | 0.36(1) | 0.57(3) | 0.45(3) | 46(3) | 0.21(1) | 1.51(1) | 0.34(2) | 33(2) | 0.31(1) | 1.04(2) | 0.28(4) | 21(3) |
| 1300 | 140 | 0.667(7) | ordered | 0.34(1) | 0.73(1) | 0.57(2) | 62(4) | 0.17(1) | 1.40(1) | 0.28(1) | 38(1) | — | — | — | — |

[a] Annealing time of experiment.
[b] Relative to $\alpha$-Fe.

at temperatures from 900 to 1320 °C for periods ranging from 40 to 1660 h in CO–$CO_2$ gas mixtures corresponding to oxygen fugacities one log unit above the iron–wüstite buffer. Under these conditions all of the iron is present as $Fe^{3+}$. Samples were drop quenched (quench rate $\sim$100 °C $s^{-1}$) and examined *ex situ* by electron microprobe analysis; compositions are reported in table 1 as mole fraction $CaFeO_{2.5}$ ($x$).

The symmetry of phases in the system $CaTiO_3$–$CaFeO_{2.5}$ was studied by means of room-temperature x-ray diffraction using a Siemens D5000 diffractometer with Cu K$\alpha$ radiation. Powdered silicon (NBS) was mixed with the sample as an internal standard, and data were analysed using the Rietveld method as implemented by the software GSAS (Larson and von Dreele 1985). Further information is given in Becerro *et al* (2000). The symbols in figure 1 show the compositions and annealing temperatures employed for the synthesis. In the region labelled 'disordered' the samples show cubic symmetry when analysed *in situ*, which excludes the possibility of long-range ordering of oxygen vacancies in the perovskite structure. Compositions near the $CaTiO_3$ endmember undergo at least two displacive phase transitions from cubic through tetragonal to orthorhombic symmetry on cooling; this phase boundary is shown as a dotted line. The displacive phase transitions involve only a change in the tilting of octahedra and are not expected to affect the arrangement of oxygen vacancies.

Samples for Mössbauer spectroscopy were prepared by mixing powdered material with benzophenone and mounting in Plexiglass sample holders. Sample weights were calculated to provide the optimum sample thickness to reduce thickness effects (Trooster and Viegers 1981, Long *et al* 1983), and varied from 0.8 to 5 mg Fe $cm^{-2}$. Mössbauer spectra were recorded in transmission mode on a constant acceleration Mössbauer spectrometer with a nominal 50 mCi $^{57}Co$ source in a 6 mm Rh matrix. The velocity scale was calibrated relative to 25 $\mu$m $\alpha$-Fe foil using the positions certified for National Bureau of Standards standard reference material No 1541; line widths of 0.28 mm $s^{-1}$ for the outer lines of $\alpha$-Fe were obtained at room temperature. Mössbauer data were collected at low temperature using a continuous flow cryostat with the sample in either nitrogen or helium vapour with a temperature uncertainty of $\pm$0.5 K. The commercially available fitting program NORMOS written by R A Brand (available from Wissenschaftliche Elektronik GmbH, Germany) was used to fit the spectra to Lorentzian and Voigt lineshapes.

For transmission electron microscopy (TEM), samples were crushed in a mortar, suspended in alcohol and then deposited on 3 mm Cu TEM grids coated with a holey amorphous carbon film. A series of compositions ranging from $x = 0.19$ to $x = 0.38$ (annealing temperature 1320 °C) were studied with a Philips CM20-FEG (field emission gun) operating at 200 kV. High-resolution TEM and selected area electron diffraction (SAED) techniques were employed to investigate changes in microstructure and crystal symmetry.

A separate set of $CaFe_xTi_{1-x}O_{3-y}$ samples was prepared for electrical conductivity measurements. Oxygen concentration is indicated in this case by a different variable, since Fe can occur as $Fe^{2+}$, $Fe^{3+}$ or $Fe^{4+}$ over the range of oxygen fugacities used during the conductivity measurements. Samples were synthesized using a method similar to that described above, and then pressed into pellets with a uniaxial pressure of 45 MPa and sintered in air at 1250 °C for 150 h. The density of the samples was >90% of the theoretical value, and scanning electron microscope measurements showed a homogeneous distribution of iron and no apparent cracks or interconnected pores. X-ray diffraction showed the samples to be single phase. An alternating current, van der Pauw four-point method was used to measure conductivities as a function of oxygen partial pressure at temperatures from 450 to 1200 °C. Conductivity was measured using a Solartron 1260 frequency response analyser operating at 123 Hz and 0.2 V amplitude. Porosity was corrected using the measured density $\rho$ and the theoretical density $\rho_{th}$ following the empirical relation $\sigma = \sigma_{meas}/(\rho/\rho_{th})^2$. The sample disc was placed at the

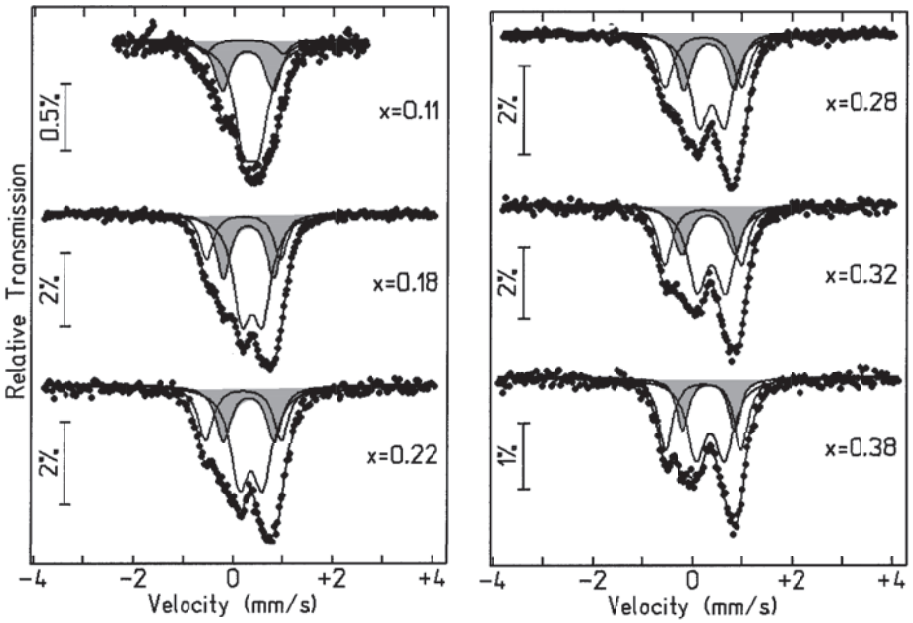


**Figure 2.** Room-temperature Mössbauer spectra of $CaFe_xTi_{1-x}O_{3-x/2}$ with different compositions annealed at 1320 °C within the disordered cubic structure region. The doublet shaded grey is assigned to pentacoordinated $Fe^{3+}$, while the unshaded doublets correspond to octahedral (small quadrupole splitting) and tetrahedral $Fe^{3+}$ (large quadrupole splitting).

open end of an $Al_2O_3$ tube that also served as an inlet for the flowing gas, and four Pt point contacts were mounted at equal distances around the rim of the top face of the sample. The entire assembly was mounted in a closed-end $Al_2O_3$ tube and inserted vertically into a tube furnace where atmosphere was controlled using one of the following gas mixtures: $O_2$ + Ar, CO + $CO_2$ or $H_2$ + $H_2O$ + Ar. The sample was held at high temperature and controlled oxygen partial pressure until conductivity values showed equilibration, and then isothermal conductivity measurements were performed at different oxygen partial pressures. Further details are given in Marion *et al* (2000).

## 3. Results

### *3.1. Mössbauer spectroscopy*

The Mössbauer spectra of samples synthesized within the cubic disordered structure region consist of several overlapping doublets (figure 2). The fitting model was chosen based on the elevated-temperature Mössbauer spectrum of the TOO phase $CaFe_{0.67}Ti_{0.33}O_{2.67}$ (Grenier *et al* 1981), which shows two well resolved quadrupole doublets indicating octahedral and tetrahedral $Fe^{3+}$. These correspond to the infinite layers of tetrahedral and octahedral sites in the fully ordered structure (Rodríguez-Carvajal *et al* 1989). As reported by Becerro *et al* (1999), spectra of the disordered phase show additional absorption—there is evidence for a third doublet (shaded grey in figure 2) with centre shift intermediate between values for octahedral and tetrahedral co-ordination. We assigned this doublet to pentacoordinated $Fe^{3+}$. All of the spectra of the cubic disordered structure were therefore fitted to three quadrupole doublets, assigned to $Fe^{3+}$ in octahedral, tetrahedral and pentacoordination. This model accounted for

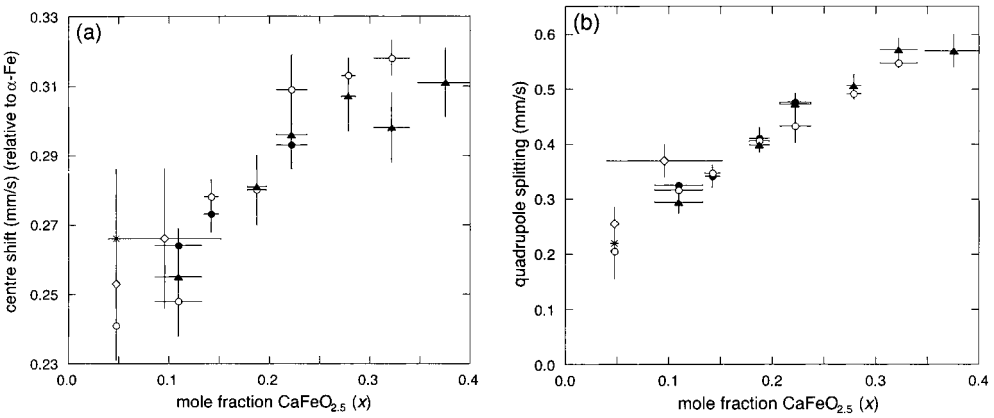


**Figure 3.** Compositional variation of (a) centre shift of pentacoordinated $Fe^{3+}$; and (b) quadrupole splitting of octahedral $Fe^{3+}$ for doublets fitted to room-temperature Mössbauer spectra of $CaFe_xTi_{1-x}O_{3-x/2}$ synthesized within the cubic disordered structure region. Symbols indicate the annealing temperatures of the samples: 900 °C (crosses); 1000 °C (open diamonds); 1100 °C (solid circles); 1200 °C (open circles) and 1320 °C (solid triangles).

all spectral absorption and no evidence for $Fe^{2+}$ or $Fe^{4+}$ was found (these would have given spectral components with significantly different centre shifts; see Hawthorne 1988). Hyperfine parameters are listed in table 1.

This is the first report of pentacoordinated $Fe^{3+}$ in the system $CaTiO_3$–$CaFeO_{2.5}$, although it has been reported using Mössbauer spectroscopy in the systems $CaFeO_{2.5}$–$CaMnO_3$ (Rodriguez *et al* 1988), $SrFeO_{2.5}$–$LaFeO_3$ (Yamamura and Kiriyama 1972) and $BaFeO_{2.5}$–$LaFeO_3$ (González-Calbet *et al* 1991). Pentacoordinated $Mn^{3+}$ has been found using neutron diffraction in the perovskite-related phases $Ba_{0.5}Sr_{0.5}MnO_{2.84}$ (Jacobson and Horrox 1976) and $CaMnO_{3-x}$ (Poeppelmeier *et al* 1982). We found pentacoordinated $Fe^{3+}$ in all of the samples that were synthesized within the region where the cubic disordered structure was stable.

The question arises as to whether pentacoordinated $Fe^{3+}$ was present in Mössbauer spectra reported by previous investigators. We digitized the spectra published by Grenier *et al* (1981) for $x = 0.02$ and $x = 0.10$ and fitted the data to the present model. Both spectra showed strong evidence for the presence of pentacoordinated $Fe^{3+}$, where values of hyperfine parameters are similar to the ones reported in table 1. There are strong qualitative indications for the presence of pentacoordinated $Fe^{3+}$ from shoulders on the peaks in the Grenier *et al* (1981) spectra, and statistically the presence of three doublets is significant to greater than the 99% level.

The centre shift and quadrupole splitting values from our Mössbauer data vary consistently with composition for all doublets and do not show significant systematic variation with temperature (table 1). Two parameters increase significantly with increasing iron concentration: the centre shift of pentacoordinated $Fe^{3+}$ (figure 3(a)) and the quadrupole splitting of octahedral $Fe^{3+}$ (figure 3(b)). Both likely indicate a change in the environment of the cation site.

The centre shift is related to the s-electron density at the nucleus, and is sensitive to the valence state of the iron atom and the geometry of the coordinating anions. Values for $Fe^{3+}$ in silicates and oxides typically fall in the ranges 0–0.25 and 0.33–0.5 mm $s^{-1}$ for tetrahedral and octahedral coordination, respectively, while the few known examples of pentacoordinated $Fe^{3+}$ fall in the range 0.22–0.34 mm $s^{-1}$ (all values relative to $\alpha$-Fe) (Burns and Solberg 1990).

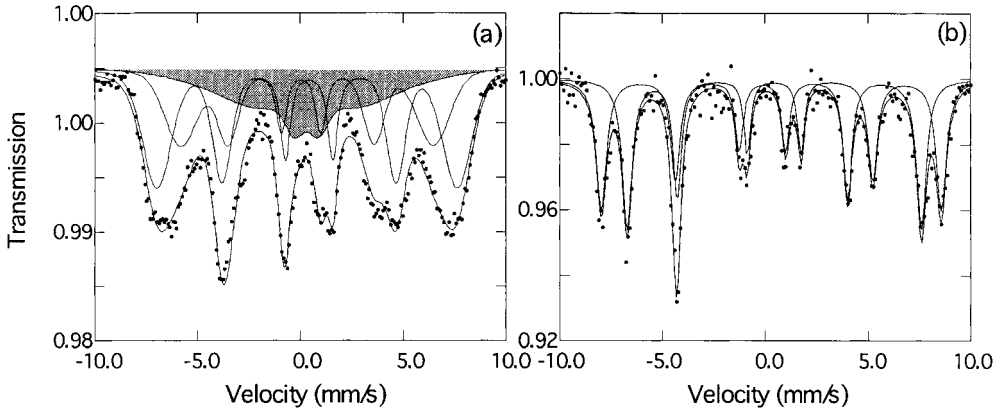


**Figure 4.** Mössbauer spectra collected at 4.2 K of (a) $CaFe_{0.38}Ti_{0.62}O_{2.81}$ which has disordered oxygen vacancies; and (b) $CaFe_{0.67}Ti_{0.33}O_{2.67}$ which has ordered oxygen vacancies. The subspectrum shaded light grey corresponds to pentacoordinated $Fe^{3+}$.

All values that we observe for pentacoordinated $Fe^{3+}$ in $CaFe_xTi_{1-x}O_{3-x/2}$ fall within the above range, including the higher values that occur at large iron concentrations.

We collected a Mössbauer spectrum of the composition $CaFe_{0.38}Ti_{0.62}O_{2.81}$ at 4.2 K (figure 4(a)) and for comparison, a spectrum of the TOO phase $CaFe_{0.67}Ti_{0.33}O_{2.67}$ (figure 4(b)). The oxygen vacancies in the structure of the latter compound are fully ordered with tetrahedral (T) and octahedral (O) layers occurring in the sequence TOO, which gives two sextets in the Mössbauer spectrum corresponding to the tetrahedral and octahedral sites. The Mössbauer spectrum of $CaFe_{0.38}Ti_{0.62}O_{2.81}$ with disordered oxygen vacancies (figure 4(a)) also shows two sextets corresponding to tetrahedral and octahedral $Fe^{3+}$, but with smaller hyperfine magnetic field and larger line broadening. These effects are probably due to variations in the next-nearest neighbour environment caused by the disordered nature of the oxygen vacancies. The presence of an additional contribution to the Mössbauer spectrum can be seen in the large amount of excess absorption near zero velocity, indicating a site with weak magnetic ordering. The hyperfine parameters cannot be uniquely determined due to uncertainty in the lineshape, but they do indicate a centre shift with value intermediate between octahedral and tetrahedral $Fe^{3+}$, probably corresponding to pentacoordinated $Fe^{3+}$ as seen in the room-temperature spectrum. The weak magnetic ordering is consistent with the isolated nature of the pentacoordinated site (see below).

### *3.2. Transmission electron microscopy*

Transmission electron microscopy (TEM) shows no evidence for ordering of oxygen vacancies in samples with compositions $x < 0.3$ that were quenched from the cubic stability field. These samples have a homogeneous, defect-free microstructure (figure 5(a)). The corresponding electron diffraction pattern (figure 5(a), inset) reveals the orthorhombic symmetry of this sample, which is due to the displacive phase transition occurring at low temperatures.

At higher Fe contents ($x > 0.3$) one observes a fine domain microtexture that is best developed at the highest Fe content ($x = 0.38$). Three sets of mutually perpendicular domains occur with size of the order of 5–10 nm (figure 5(b)). The corresponding electron diffraction pattern on this scale (figure 5(b), inset) represents a superposition of the diffraction contributions from the three differently oriented domains, each with orthorhombic symmetry.

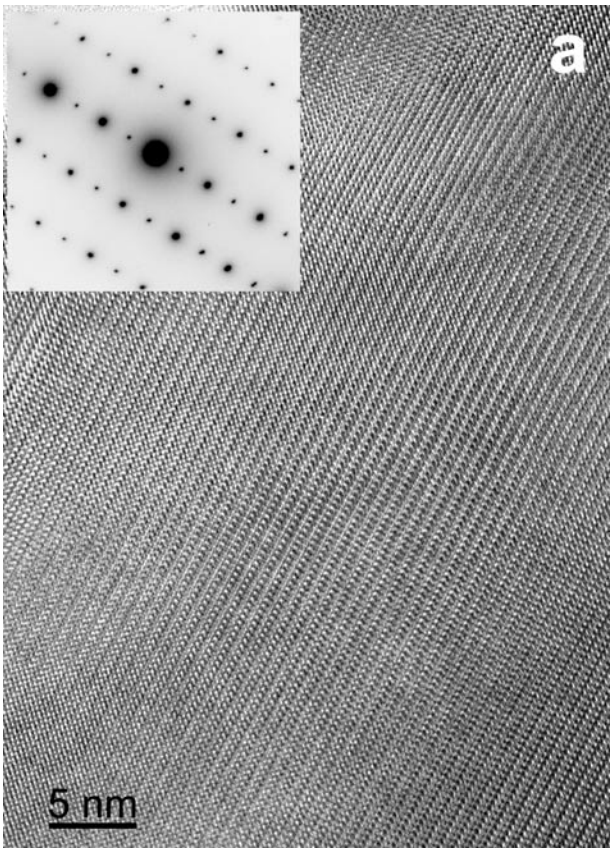


**Figure 5.** High-resolution TEM micrographs and SAED patterns of (a) $CaFe_{0.19}Ti_{0.81}O_{2.81}$ showing a homogeneous microtexture and orthorhombic symmetry; and (b) $CaFe_{0.38}Ti_{0.62}O_{2.90}$ showing slight ordering of oxygen vacancies in domains that occurred during quenching.

In addition to the superposition phenomena, the diffraction patterns display diffuse streaks in the *a* directions of the former cubic structures. As in a previous study (Becerro *et al* 1999) we attribute the presence of these streaks to partial ordering of oxygen vacancies which causes the symmetry to be orthorhombic. The partial ordering process probably occurred during quenching when the samples passed through the stability field of the partially ordered phases. At higher Fe contents this field extends to higher temperatures (figure 1) where the kinetics of the reaction are faster.

XRD results show the same sample ($x = 0.38$) to have cubic symmetry, which we attribute to the nature of the domains. Their small size as well as the likely permanent strain between domains oriented in mutually perpendicular directions gives an average over the bulk structure that is metrically cubic. Diffraction lines in the x-ray pattern are significantly broadened at these compositions, consistent with this interpretation.

The partial ordering in the $x = 0.38$ sample does not reduce significantly the proportion of pentacoordinated $Fe^{3+}$, where Mössbauer spectroscopy shows a similar relative abundance compared to spectra from samples with smaller values of $x$ (table 1). While the microstructure seen in figure 5(b) implies partial ordering of tetrahedral and octahedral sites into layers, the short timescale of the quenching process probably results in some disorder within the ordered

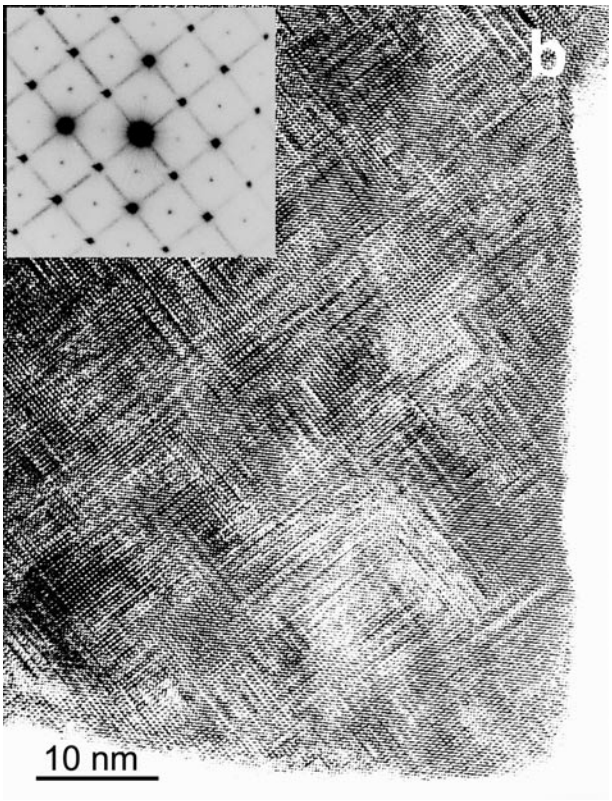


**Figure 5.** (Continued)

regions. Pentacoordinated $Fe^{3+}$ would then occur not only along intersection planes, but also within the layers.

### *3.3. Electrical conductivity*

Conductivity isotherms of $CaFe_xTi_{1-x}O_{3-y}$ for $x = 0.1$ can be interpreted in terms of n-type, ionic and p-type conduction at low, intermediate and high oxygen fugacities, respectively (Marion *et al* 2000). Our new data show that this is also true for $x = 0.2$ and $x = 0.3$. In the range where ionic conductivity predominates we expect that Fe is present nearly exclusively as $Fe^{3+}$, which is the range for which the phase diagram in figure 1 is valid. The ionic part of the conductivity can be derived from the variation of conductivity with oxygen fugacity at constant temperature and is plotted in figure 6. Data for $x = 0.1$ show a consistent trend over all temperatures, consistent with the phase diagram which shows no oxygen vacancy ordering at $T > 900\,^{\circ}C$ (figure 1). In contrast, data for $x = 0.2$ show a discontinuity near $1000\,^{\circ}C$ that probably corresponds to the order–disorder phase transition. Ionic conductivity data for $x = 0.3$ show a sharp decrease from a high value at $1200\,^{\circ}C$ (which corresponds to the disordered region of the phase diagram) to a lower value at $1100\,^{\circ}C$ (which lies below the order–disorder phase transition). Our data are consistent with those of Dunyushkina *et al* (1999) who found that $CaFe_xTi_{1-x}O_{3-y}$ with $x = 0.2$ showed the highest oxygen ion conductivity at temperatures of 1000–$1100\,^{\circ}C$.

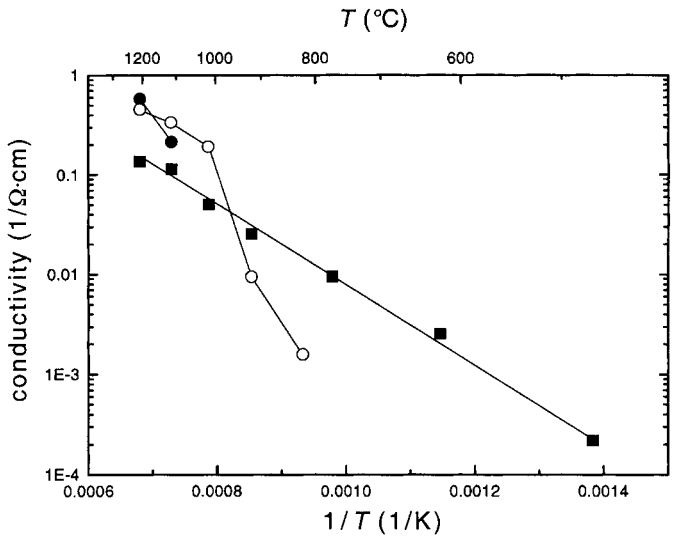


**Figure 6.** Variation of ionic conductivity with inverse temperature for $CaFe_xTi_{1-x}O_{3-x/2}$ with nominal composition $x = 0.1$ (squares), $x = 0.2$ (open circles) and $x = 0.3$ (closed circles). The solid lines are provided as a guide to the eye.

## 4. Discussion

### *4.1. Cation site distribution*

In Mössbauer spectroscopy, the relative area of a subspectrum is related to the relative abundance of the corresponding crystallographic site, and to a first approximation the two can be considered equal. The relative area fractions listed in table 1 therefore give an indication of the relative abundance of Fe in the octahedral, tetrahedral and pentacoordinated sites.

The Mössbauer effect sees only Fe, but we must consider that the B cation sites are also occupied by Ti. Grenier *et al* (1981) assumed that Ti occupies only octahedral sites within the system $CaTiO_3$–$CaFeO_{2.5}$, but the Mössbauer data can be used to test this assumption directly. When Fe is present only in the 3+ state and Ti is assumed to always be in the 4+ state, we can calculate the number of oxygen vacancies directly from the iron content based on the assumption of electroneutrality. Figure 7 shows a comparison of this value with the one calculated from the Mössbauer data, based on one oxygen vacancy per tetrahedral site and a half oxygen vacancy per pentacoordinated site assuming that Ti occupies only the octahedral sites. There is a systematic offset from the 1:1 correlation line.

It is worthwhile at this point to review the assumptions made in determining the relative site occupancies from the area fractions in the Mössbauer data. These include effects due to differences in recoil-free fraction between the different sites, and thickness effects. To investigate the first effect, we recorded the Mössbauer spectrum of $CaFe_{0.38}Ti_{0.62}O_{2.81}$ at 80 K where effects from differing recoil-free fractions are significantly smaller than at 293 K. Results were identical to those at 293 K within experimental error (figure 7), indicating that the systematic offset is not due to differences in recoil-free fractions between sites. The offset cannot be due to thickness effects either, since they cause an overestimate of the less abundant components in the Mössbauer spectrum. In our case these are the components corresponding to tetrahedral and pentacoordinated $Fe^{3+}$, so correction for thickness effects would cause a greater departure of the data from the 1:1 correlation line. We note that thickness effects

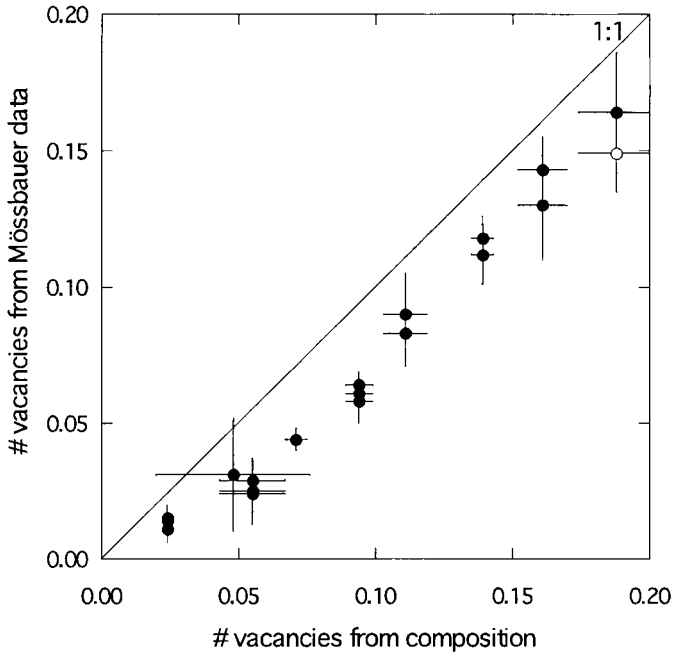


**Figure 7.** Comparison of the number of oxygen vacancies per formula unit calculated from the iron concentration with the number determined from the Mössbauer data, assuming that Ti occupies only octahedral sites. Solid circles indicate data collected at 293 K, while the open circle indicates data collected at 80 K. The systematic offset of the data from the 1:1 correlation line is probably due to the presence of a small amount of Ti on non-octahedral sites.

should not be evident in our data in any event, since experimental absorber thicknesses were deliberately chosen to minimize these effects.

The most likely possibility for the systematic offset of the data from the 1:1 line in figure 7 is that some Ti is located on the pentacoordinated and/or the tetrahedral sites. Determinations of unique site distributions are only possible if we assume that Ti occupies one other site, so for reasons that are outlined in the following section, we assume that Ti is distributed over the octahedral and pentacoordinated sites only. In this case the exchange of Ti and Fe between the octahedral (O) and pentacoordinated (P) sites is represented by the following equation:

$$Ti^{4+}(P) + Fe^{3+}(O) = Ti^{4+}(O) + Fe^{3+}(P). \tag{1}$$

We can calculate the partition coefficient $K_D$ $(= (O_{Ti}P_{Fe})/(P_{Ti}O_{Fe}))$ as a function of composition and temperature using the number of oxygen vacancies calculated from the iron concentration combined with the iron site abundance from the Mössbauer data. Results plotted as a function of composition (figure 8(a)) indicate that the partition coefficient increases with increasing Fe concentration, implying that the relative proportion of Ti occupying pentacoordinated sites is lower at high oxygen vacancy concentrations. There also appears to be a trend in $K_D$ with temperature, which can be more easily seen if we average the partition coefficient data over all compositions for each temperature (figure 8(b)). At higher temperatures there is a greater partitioning of Ti onto the pentacoordinated sites. The partition coefficients in figure 8 are quite high, indicating that the largest proportion of Ti is on octahedral sites.

It is also possible that a small proportion of Ti could occupy tetrahedral sites. This would have a similar effect to reduce the systematic offset from the 1:1 correlation line in figure 7,

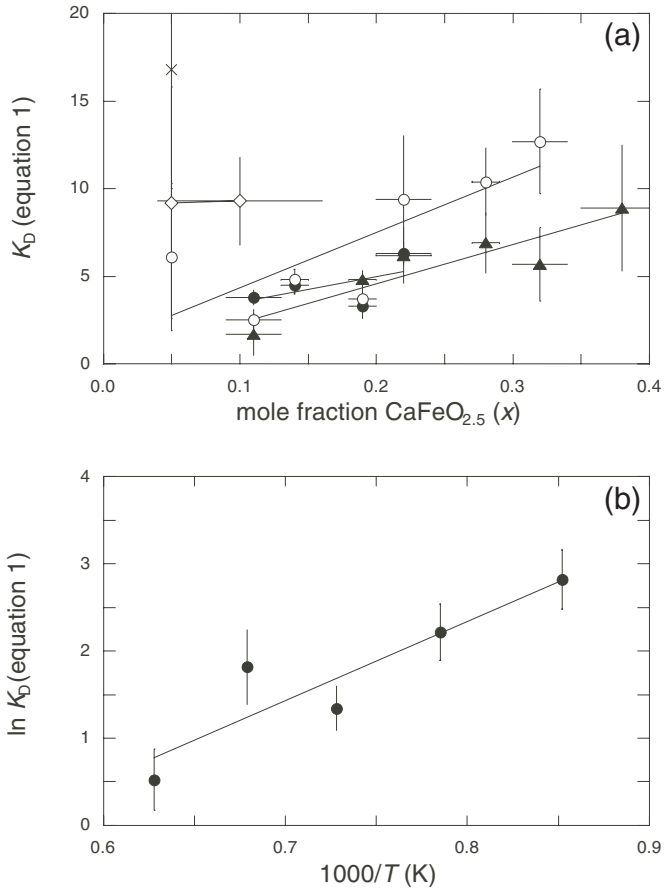


**Figure 8.** (a) Variation of $K_D$ (where $K_D = (O_{Ti}P_{Fe})/(P_{Ti}O_{Fe})$) with composition for $CaFe_xTi_{1-x}O_{3-x/2}$ synthesized within the cubic disordered structure region. Ti is assumed to occupy only the octahedral and pentacoordinated sites. Symbols indicate the annealing temperatures of the samples: 900 °C (crosses); 1000 °C (open diamonds); 1100 °C (solid circles); 1200 °C (open circles) and 1320 °C (solid triangles). Solid lines indicate linear fits to the data from individual temperatures. (b) Inverse temperature variation of ln $K_D$ averaged over all compositions. The solid line indicates a linear fit to the data.

except that half the number of Ti atoms would be needed because the number of oxygen vacancies involved would be doubled. If Ti occupied all three sites, it would not be possible to uniquely determine partition coefficients from our data. We emphasize, however, that since the total number of non-octahedral Ti atoms implied by figure 7 is relatively small, partitioning of Ti between the pentacoordinated and tetrahedral sites would have only a minor effect on the results and our conclusions would remain the same.

Mössbauer data from the fully ordered TOO phase $CaFe_{0.67}Ti_{0.33}O_{2.67}$ can also be used to determine the amount of Ti on non-octahedral sites. From our spectrum at 4.2 K (figure 4(b)) the area ratios for the octahedral and tetrahedral sites give a ratio O/T of $0.94 \pm 0.06$. If Ti were present on any of the tetrahedral sites, O/T would be greater than 1.0 since Ti is invisible to the Mössbauer effect. We therefore conclude that Ti is only located in octahedral sites in the TOO phase. This is consistent with the increase in partition coefficient with Fe concentration seen in figure 8(a).

**Table 2.** Cation site distribution in $CaFe_xTi_{1-x}O_{3-x/2}$ determined from 293 K Mössbauer data and chemical composition.

| $T$ (°C) | $x$ | $O_{Fe}$ | $T_{Fe}$ | $P_{Fe}$ | $O_{Ti}$[a] | $P_{Ti}$[a] |
|---|---|---|---|---|---|---|
| 900 | 0.048(4) | 0.0256(29) | 0.0081(18) | 0.0139(28) | 0.9349(24) | 0.0175(24) |
| 1000 | 0.048(4) | 0.0236(28) | 0.0045(19) | 0.0195(28) | 0.9332(25) | 0.0192(25) |
| | 0.096(56) | 0.0552(46) | 0.0205(24) | 0.0200(50) | 0.8696(39) | 0.0347(39) |
| 1100 | 0.110(23) | 0.0676(14) | 0.0159(10) | 0.0260(14) | 0.8389(14) | 0.0516(14) |
| | 0.142(7) | 0.0779(18) | 0.0237(13) | 0.0405(18) | 0.8038(19) | 0.0541(19) |
| | 0.188(10) | 0.1043(54) | 0.0334(36) | 0.0499(57) | 0.7415(57) | 0.0709(57) |
| | 0.222(15) | 0.1110(29) | 0.0548(20) | 0.0565(33) | 0.7215(33) | 0.0562(33) |
| 1200 | 0.048(4) | 0.0313(31) | 0.0054(22) | 0.0109(30) | 0.9265(28) | 0.0259(28) |
| | 0.110(23) | 0.0743(25) | 0.0137(18) | 0.0215(23) | 0.8299(24) | 0.0606(24) |
| | 0.142(7) | 0.0784(21) | 0.0249(19) | 0.0388(20) | 0.8044(24) | 0.0535(24) |
| | 0.188(10) | 0.0994(48) | 0.0330(36) | 0.0552(51) | 0.7460(55) | 0.0664(55) |
| | 0.222(15) | 0.0942(102) | 0.0514(67) | 0.0767(117) | 0.7349(115) | 0.0428(115) |
| | 0.279(7) | 0.1217(48) | 0.0791(36) | 0.0781(57) | 0.6785(64) | 0.0426(64) |
| | 0.322(18) | 0.1370(53) | 0.1002(42) | 0.0849(67) | 0.6411(79) | 0.0368(79) |
| 1320 | 0.110(23) | 0.0689(47) | 0.0085(34) | 0.0322(45) | 0.8301(46) | 0.0604(46) |
| | 0.188(10) | 0.0971(26) | 0.0373(20) | 0.0532(28) | 0.7526(30) | 0.0598(30) |
| | 0.222(15) | 0.1120(77) | 0.0548(56) | 0.0555(89) | 0.7205(92) | 0.0572(92) |
| | 0.279(7) | 0.1310(77) | 0.0753(56) | 0.0726(90) | 0.6653(100) | 0.0558(100) |
| | 0.322(18) | 0.1525(125) | 0.0896(95) | 0.0800(154) | 0.6149(180) | 0.0630(180) |
| | 0.376(28) | 0.1728(115) | 0.1256(89) | 0.0773(125) | 0.5770(175) | 0.0473(175) |

$O$, $T$ and $P$ refer to the proportion of cations on the octahedral, tetrahedral and pentacoordinated sites, respectively.
[a] Assuming that all non-octahedral Ti is located on pentacoordinated sites.

We can use the Mössbauer data combined with the oxygen vacancy concentration calculated from the iron concentration to determine the cation site distribution in $CaFe_xTi_{1-x}O_{3-x/2}$ as a function of composition and temperature, assuming that Ti occupies octahedral and pentacoordinated sites. These results are listed in table 2.

We note that the Mössbauer data does not provide information about whether there is ordering of Ti and Fe atoms on the octahedral sites. Grenier *et al* (1981) saw evidence for two different types of $Fe^{3+}$ octahedral site, which they ascribed to differences in the next-nearest neighbours. The ratio of the two octahedral sites was close to 2:1, which would be consistent with a random distribution of Ti and Fe within the layers. This is not a unique interpretation of the data, however, so the question of Fe/Ti ordering remains open.

### *4.2. Local structure and short-range ordering of oxygen vacancies*

We propose the following model to describe the development of short-range ordering of oxygen vacancies in $CaFe_xTi_{1-x}O_{3-x/2}$. It is based on the model already described by Becerro *et al* (1999) and incorporates new results from the present work. Following the well known mechanism (written in Kröger–Vink notation; Kröger and Vink 1956)

$$Fe_2O_3 + 2Ti_{Ti} + O_O \rightarrow 2Fe'_{Ti} + V_O^{\cdot\cdot} + 2TiO_2 \qquad (2)$$

Ti on octahedral sites in $CaTiO_3$ is replaced by $Fe^{3+}$, forming oxygen vacancies to balance charge. The introduction of the first two Fe atoms results in the formation of two pentacoordinated sites and a monomer (a single oxygen vacancy) (figure 9), where the pentacoordinated sites would be occupied by Fe and Ti on the basis of entropy considerations, and the other Fe atom would replace Ti on an octahedral site. The presence of pentacoordinated Ti is consistent with our results described above.

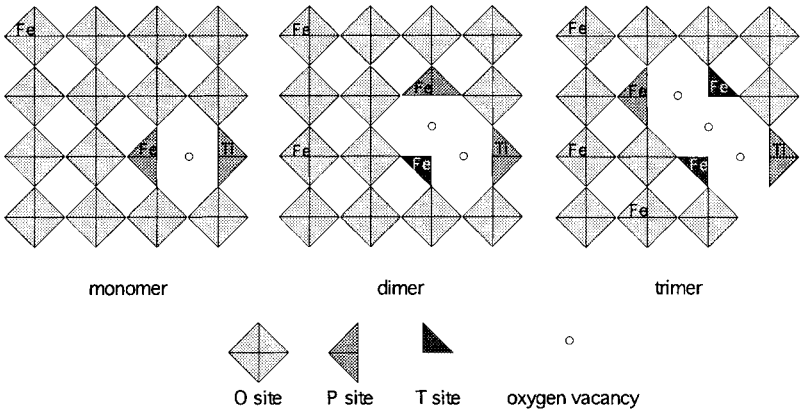


**Figure 9.** Projection of the cubic structure projected onto the (0$k$0) plane showing the growth of an oxygen vacancy chain along [101] (after Becerro *et al* 1999).

A dimer can be formed with the substitution of two more Fe atoms, forming a tetrahedral site plus the two original pentacoordinated sites (figure 9). As for the monomer case above, one Fe atom would probably be associated with the oxygen vacancy (in this case the tetrahedral site), while the other would replace Ti on an octahedral site.

A trimer can be formed with the substitution of two more Fe atoms, but in this case there is a choice of position, forming either a linear or a kinked chain. The straight configuration is expected to be energetically more favourable because a kinked growth of defects would result in a very low coordination number for the A site (Komornicki *et al* 1981). As above, one Fe atom would be associated with the new tetrahedral site, while the other would replace Ti on an octahedral site. In this way the proportion of Fe on octahedral sites should remain roughly 50% of the total number of sites occupied by Fe, which is consistent with our Mössbauer data (table 1).

The addition of further oxygen vacancies would increase the number of tetrahedral sites while the number of pentacoordinated sites remains constant (one at each end of the chain). It is straightforward to calculate the average number of vacancies per chain from the relative proportions of tetrahedral ($T$) and pentacoordinated ($P$) sites:

$$N = \frac{2-a}{a} \qquad \text{where } a = \frac{P}{P+T}. \tag{3}$$

We have calculated the average chain length based on the Mössbauer data (table 1) and the Ti partitioning data (figure 8), and results show a nearly linear increase in chain length with increasing Fe concentration (figure 10). Since the minimum number of vacancies per chain is one, samples with low iron concentration at high temperature must contain a high proportion of monomers. This is not true at lower temperatures (900–1000 °C), however, where the average number of vacancies per chain is higher.

We can now interpret the decreasing proportion of Ti on pentacoordinated sites (figure 8(a)) based on the results in figure 10. When $x$ is small and the number of monomers is high, the proportion of Ti on pentacoordinated sites must also be high since Fe–Fe pairs in adjacent pentacoordinated sites would not be favoured due to entropy considerations. As the length of vacancy chains increases, however, the relative proportion of Ti on pentacoordinated sites would decrease, consistent with the trend shown in figure 8(a). It is important to note that because the total number of Ti atoms on non-octahedral sites is small, our conclusion that the average chain length increases with increasing Fe concentration is independent of assumptions

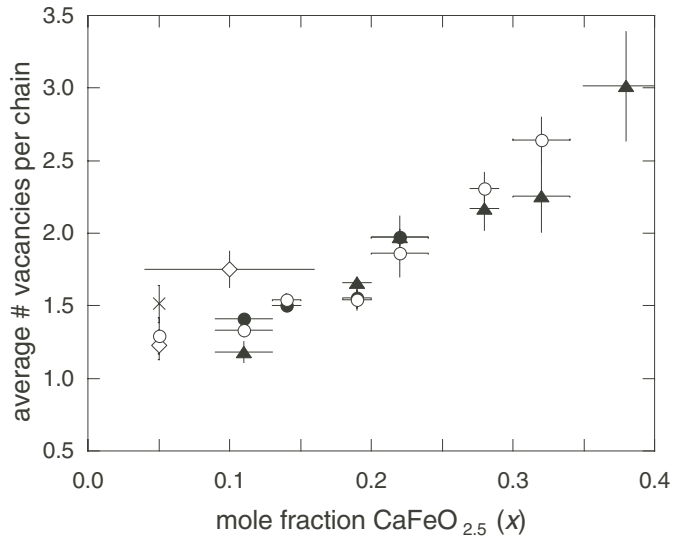


**Figure 10.** Compositional variation of the average number of oxygen vacancies per chain in $CaFe_xTi_{1-x}O_{3-x/2}$ calculated from the site abundance data assuming that Ti is distributed over both octahedral and pentacoordinated sites. Symbols indicate the annealing temperatures of the samples: 900 °C (crosses); 1000 °C (open diamonds); 1100 °C (solid circles); 1200 °C (open circles) and 1320 °C (solid triangles).

about Ti partitioning. A similar result is obtained if Ti is assumed to occupy only the octahedral sites.

We can now interpret the increase in quadrupole splitting of the octahedral site with increasing Fe concentration (figure 3(b)) in terms of our model. At low vacancy concentrations, octahedral sites containing Fe are surrounded by other octahedral sites, and the low distortion of the octahedral environment results in low quadrupole splitting. As the number of oxygen vacancies and the average chain length increase, however, the probability of an octahedral site being adjacent to either a pentacoordinated or tetrahedral site also increases. This produces a larger distortion of the octahedral site and hence a larger quadrupole splitting. In contrast, we note that the quadrupole splitting of the pentacoordinated and tetrahedral sites is approximately constant (table 1), which is consistent with the smaller variation in next-nearest-neighbour environment of these sites with increasing oxygen vacancy concentration.

We note that the average vacancy chain length calculated from the Mössbauer data is not necessarily appropriate for samples where partial ordering of vacancies occurred during the quenching process. In this case pentacoordinated $Fe^{3+}$ arises not only from termination of vacancy chains, but also from intersection of vacancy layers. However, TEM observations showed the presence of partial ordering only in the samples with the highest Fe concentrations, so we do not consider this effect to be relevant for the remainder of our dataset.

We can also interpret the electrical conductivity data (figure 6) in terms of our model. The high ionic conductivity in the system is probably due to the high proportion of monomers which enables a high mobility of oxygen vacancies. At constant temperature, ionic conductivity values increase with increasing $x$ due to the higher concentration of oxygen vacancies, but this effect is offset by the increasing length of vacancy chains which enhances the tendency to trap vacancies and reduce their mobility. This can be used to explain the sequence of ionic conductivity values at 1200 °C, where there is a large jump from $x = 0.1$ to 0.2, but only a

slight increase in ionic conductivity from $x = 0.2$ to 0.3. The values of ionic conductivity measured below 900 °C probably reflect supercooling of the disordered configuration since kinetics of the ordering process are probably slow (Marion *et al* 2000).

## Acknowledgments

A portion of the research was supported through the EU TMR Network programme (ERB-FMRX-CT97-0108). Mössbauer experiments were performed with the help of equipment purchased with funds awarded to F Seifert by Fonds der Chemischen Industrie (Germany) under the 'Materials Research' programme.

## References

Becerro A I, Angel R, McCammon C A, Langenhorst F and Seifert F 2000 *J. Phys.: Condens. Matter* at press

Becerro A I, McCammon C A, Langenhorst F, Seifert F and Angel R 1999 *Phase Transitions* **69** 133–46

Burns R G and Solberg T C 1990 *Spectroscopic Characterization of Minerals and their Surfaces* vol 415, eds L M Coyne, S W S McKeever and D F Blake (Washington, DC: American Chemical Society) pp 262–83

Colville A A 1970 *Acta Crystallogr.* B **26** 1469–73

Dunyushkina L A, Demin A K and Zhuravlev B V 1999 *Solid State Ion.* **116** 85–8

González-Calbet J M, Parras M, Vallet-Regí M and Grenier J C 1991 *J. Solid State Chem.* **92** 110–15

Grenier J C, Pouchard M and Hagenmuller P 1981 *Struct. Bonding* **47** 1–25

Hawthorne F C 1988 *Spectroscopic Methods in Mineralogy and Geology* ed F C Hawthorne (Washington, DC: Mineralogical Society of America) pp 255–340

Hovmöller S, Zou X D, Wang N, González-Calbet J M and Vallet-Regí M 1988 *J. Solid State Chem.* **77** 316–21

Iwahara H, Esaka T and Mangahara T 1988 *J. Appl. Electrochem.* **18** 173–7

Jacobson A J and Horrox A J W 1976 *Acta Crystallogr.* B **32** 1003–8

Komornicki S, Grenier J C, Pouchard M and Hagenmuller P 1981 *Nouv. J. Chim.* **5** 161–6

Kröger F and Vink H 1956 *Solid State Physics* ed F Seitz and D Turnbull (New York: Academic) pp 307–435

Larson A C and von Dreele R B 1985 General Structure Analysis System (GSAS) *Los Alamos National Laboratory Report* LAUR B6-748

Long G L, Cranshaw T E and Longworth G 1983 *Möss. Effect Ref. Data J.* **6** 42–9

Marion S, Becerro A I and Norby T 1999 *Phase Transitons* **69** 157–68

——2000 *Ionics* at press

Poeppelmeier K R, Leonowicz M E, Scanlon J C and Longo J M 1982 *J. Solid State Chem.* **45** 71–9

Rodriguez J, Fontcuberta J, Longworth G, Vallet-Regí M and González-Calbet J M 1988 *J. Solid State Chem.* **73** 57–64

Rodríguez-Carvajal J, Vallet-Regí M and González-Calbet J M 1989 *Mater. Res. Bull.* **24** 423–30

Trooster J M and Viegers M P A 1981 *CRC Handbook of Spectroscopy* vol 3, ed J W Robinson (Boca Raton, FL: Chemical Rubber Company) pp 465–76

Yamamura H and Kiriyama R 1972 *Bull. Chem. Soc. Japan* **45** 2701–8